

VIGFace: Virtual Identity Generation Model for Face Image Synthesis

Minsoo Kim^{*1,2} , Min-Cheol Sagong^{*1} , Gi Pyo Nam^{1,2} , Junghyun Cho^{1,2,3} , and Ig-Jae Kim^{1,2,3} 

¹ Korea Institute of Science and Technology, Korea

² Korea National University of Science and Technology, Korea

³ Yonsei-KIST Convergence Research Institute, Yonsei University
{kim1102, mcsagong, gpnam, jhcho, drjay}@kist.re.kr

Abstract. Deep learning-based face recognition continues to face challenges due to its reliance on huge datasets obtained from web crawling, which can be costly to gather and raise significant real-world privacy concerns. To address this issue, we propose **VIGFace**, a novel framework capable of generating synthetic facial images. Initially, we train the face recognition model using a real face dataset and create a feature space for both real and virtual IDs where virtual prototypes are orthogonal to other prototypes. Subsequently, we generate synthetic images by using the diffusion model based on the feature space. Our proposed framework provides two significant benefits. Firstly, it allows for creating virtual facial images without concerns about portrait rights, guaranteeing that the generated virtual face images are clearly differentiated from existing individuals. Secondly, it serves as an effective augmentation method by incorporating real existing images. Further experiments demonstrate the efficacy of our framework, achieving state-of-the-art results from both perspectives without any external data.

Keywords: Face recognition, Diffusion model, Image generation, Data augmentation, Synthetic data

1 Introduction

Deep learning-based Face Recognition (FR) models have significantly improved their performance due to recent advancements in network architectures [16, 17, 20, 25, 46, 48] and enhancements in loss functions [10, 27, 30, 43, 44, 54]. The latest FR models utilize the softmax-variant loss for training to reduce intra-class variance and increase inter-class separability in the embedding space. This necessitates a very large dataset with numerous distinct individuals, significant variations within each individual for intra-class variance, and precise labels of subject identities (IDs). However, the datasets are typically collected through web-crawling and then refined using automatic techniques that employ FR logs [9, 58]. While this approach is successful in eliminating mislabeled data, it

* These authors contributed equally to this work

still struggles with persistent issues of small intra-class variance. Moreover, in the face recognition field, unlike other ordinary image classifications, there are practical issues such as portrait rights, making it even more difficult to collect training data. For instance, datasets such as those referenced in [15,55,58] consist of images of celebrities crawled from the internet without consent. Additionally, datasets mentioned in [26,37] include facial images of the general populace, including children. After facing strong criticism, public access to these datasets has been revoked [52].

Synthetic datasets have been employed to overcome limitations caused by a scarcity of real datasets [8, 24, 51] and biases present in the available real datasets [6, 19]. In the realm of face recognition, artificial faces show promise in addressing the aforementioned issues related to real face datasets. Generated faces have low risk from label noise due to conditional generation. Bias problems such as long-tailed distributions, which lead to class imbalances, can be mitigated by data augmentation. Importantly, there are no privacy concerns with facial images of virtual identities if the method is effective. Therefore, when creating artificial datasets, it is essential to consider: 1) ensuring the generated data mirrors real data distribution, 2) enhancing ability to generate new subjects in the target domain by taking the full source domain into account for augmentation, and 3) maintaining ID consistency for each subject.

Previous attempts to create artificial face datasets have addressed some of the three aspects individually, but to the best of our knowledge, none have simultaneously taken into account all three aspects [2, 28, 39]. SynFace [39] introduces a high-quality synthetic face image dataset, closely resembling real face images, using DiscoFaceGAN [12]. Nonetheless, DiscoFaceGAN is only capable of generating a limited number of unique subjects, fewer than 500 [28]. On the other hand, DigiFace [2] utilizes 3D parametric modeling to create synthetic face images of various subjects. However, it faces difficulties in accurately replicating the quality and style distribution observed in real face images. DCFace [28] proposes a diffusion-based method for generating data that can produce a large number of novel subjects, maintain the style of real datasets, and ensure label consistency. However, DCFace primarily focuses on creating synthetic data rather than increasing the capabilities of data augmentation.

We present a novel approach for generating face data that enhances both intra-class variance and inter-class diversity. The main concept of our paper is incorporating virtual prototypes into the FR model. The diffusion model is trained to preserve the identity of the individuals when generating face images based on the FR embedding. Since virtual prototypes are orthogonal to other prototypes, virtual subjects are guaranteed to be distinguished from the original data. Fig. 1 shows toy example visualizing the embeddings of real and virtual subjects to demonstrate the effectiveness of the suggested method. The virtual embedding can be distinct from the real individual clusters, whereas the images generated from virtual prototypes form unique clusters. The visualization demonstrates that our framework generates distinctive virtual human faces with high ID consistency. The proposed method effectively addresses privacy concerns by creating

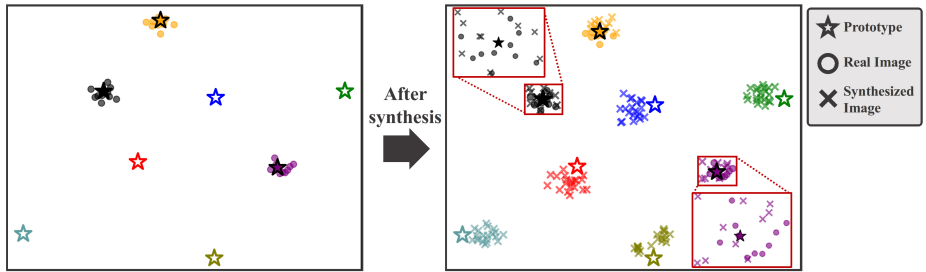


Fig. 1: T-distributed Stochastic Neighbor Embedding (T-SNE) [33] plot of embeddings from real and synthesized images. The filled and lined stars represent the real and virtual prototypes, while circles and crosses indicate the position for embeddings of real and synthesized images, respectively.

datasets of non-existent individuals and achieving state-of-the-art performance compared to models trained with previous virtual person generation methods. Additionally, the FR model, which was trained using combination of real and synthetic images together, achieves better performance than the model trained using only real images. This shows that the proposed method is also superior from the perspective of a data-augmentation method. Our contribution can be summarized as follows:

- Proposing VIGFace, a solution capable of generating virtual face images that addresses three important criteria for face recognition: realistic appearance, novel subjects, and consistent ID characteristics.
- Showing that the synthetic data generated by our proposed method can enhance intra-class and inter-class variance by achieving SOTA performance in face recognition.
- Releasing the first virtual-only face dataset that can fully substitute the real dataset, aiding in alleviating privacy concerns.

2 Related work

2.1 Face Recognition Models

Current SOTA FR methods, such as [4, 10, 11, 23, 27, 30, 34, 53], are designed based on the softmax loss but particularly utilize angular/cosine distance instead of Euclidean distance. The goal of these methods is to maximizing the similarity between the embeddings and the ground-truth (GT) prototype while minimizing the similarity between the embedding and prototypes of other classes. As a result, all embeddings in the same class, including prototypes, converge while maintaining their maximum distance from other classes. Therefore, if the embedding dimension is large enough, the clusters of each class will be nearly orthogonal [10]. Naturally, a dataset that is larger and contains a greater various of images allows for the training of better-performing FR models. Therefore,

over time, larger and more diverse datasets [1, 15, 21, 58] have been collected and published in the academic field. However, issues such as portrait rights and the high cost of building large-scale data still remain unresolved.

2.2 Synthetic Face Image Generation

Synthetic training datasets have demonstrated advantages in areas such as face recognition [2, 39] and anti-spoofing [31, 49]. They can address class imbalance issues related to informed consent and racial biases that often noted in conventional large-scale face datasets [2, 10, 39]. Moreover, they endorse the importance of ethical considerations, like portrait rights. Despite their benefits, the use of synthetic datasets lacks widespread acceptance, causing reduced recognition accuracy when employed as the sole training data.

SynFace [39] proposed the method using DiscoFaceGAN [12] to synthesize the virtual face. DigiFace-1M [2] suggested 3D model-based face rendering with image augmentations to create virtual face data and showed that the FR model could be trained using only virtual face images. DCFace [28] proposed a diffusion-based face generator combining subject appearance (ID) and external factor (style) conditions. Although the above images have succeeded in reducing the dependence on images crawled from the web, there is still a performance gap between the FR model trained on real training datasets and the FR model trained on synthetic training datasets. We proposed a data augmentation method that can generate the virtual ID with high intra-class variance and large number of unique individuals, thereby aiding in FR model training.

3 Preliminary

3.1 Diffusion Model

Diffusion model gradually denoises random Gaussian noise to generate real data. The diffusion model reverses the forward noise-injection process, also called diffusion process, which is formulated as a Markov chain:

$$q(x_{1:T}|x_0) = \prod_{t=1}^T q(x_t|x_{t-1}), \quad (1)$$

where x_0 is real data, $q(x_t|x_{t-1}) = \mathcal{N}(x_t; \sqrt{1 - \beta_t}x_{t-1}, \beta_t I)$, and β_t is the differentiable noise schedule. To reverse this process, also called denoising process, the diffusion model is learned to denoise $x_t \sim q(x_t|x_0)$ into an estimate $\hat{x}_\theta(x_t, t) \approx x_0$ for all t that are uniform between 1 and T . Formally, this is achieved by training \hat{x}_θ using squared error loss:

$$\min_{\theta} \mathbb{E}_{\epsilon, t} \|\hat{x}_\theta(x_t, t, c) - x_0\|_2^2, \quad (2)$$

where c is an optional conditioning label or its continuous embedding vector. Recent work shows that c can be from various modalities such as a low-resolution image or text embedding [41, 42].

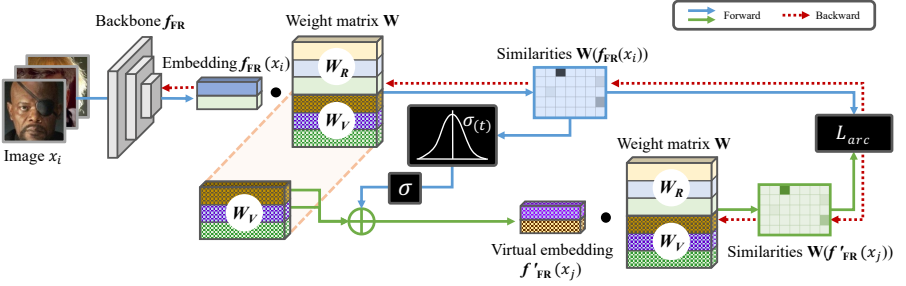


Fig. 2: Pipeline for stage 1: suggesting face recognition model training. Conventional FR training includes prototypes for real individuals only, denoted as $W_R = [w_r^1, w_r^2, \dots, w_r^n]$. We add k prototypes for virtual IDs, denoted as $W_V = [w_v^1, w_v^2, \dots, w_v^k]$.

4 Methods

Our framework comprises two stages. Firstly, we train the FR model using the real face dataset and design the feature space for both real and virtual IDs. Subsequently, synthetic images are generated using the diffusion model based on the feature space of a pre-trained FR model. This section provides a detailed explanation of each component of the proposed framework.

4.1 Stage 1: FR Model Training

The proposed framework begins with training the FR model using real face images. The overall pipeline of this stage is illustrated in Fig. 2. This stage serves two purposes: 1) Training the FR model to extract ID embeddings from face images, which are necessary for training the diffusion model in the second stage, and 2) Simultaneously assigning the positions of both the real ID and the virtual ID on the feature space. We choose ArcFace [10] to train the FR model in this stage. The ArcFace loss used to train the FR backbone f_{FR} and the prototype $W = [w_1, w_2, \dots, w_n]$ can be described as follows:

$$L_{arc} = -\log \frac{e^{s \cos(\theta_{y_i} + m)}}{e^{s \cos(\theta_{y_i} + m)} + \sum_{j=1, j \neq y_i}^n e^{s \cos \theta_j}}, \quad (3)$$

$$\cos \theta_j = \frac{w_j^T f_{FR}(x_i)}{\|w_j\| \|f_{FR}(x_i)\|}, \quad (4)$$

where n denotes the total number of real IDs, while m and s represent the margin and scale hyperparameters, respectively. With conventional FR training methods, only prototypes for real individuals, that can be denoted as $W_R = [w_r^1, w_r^2, \dots, w_r^n]$, are necessary for training. However, in our work, we include additional k prototypes for virtual IDs, denoted as $W_V = [w_v^1, w_v^2, \dots, w_v^k]$, which are used to generate facial images of non-existent individuals. As a result, the

prototype is defined as a linear transformation matrix $W \in \mathbb{R}^{(n+k) \times D}$, where D refers to the dimension of the embedding features.

However, due to the absence of a face image for virtual IDs, their prototypes cannot be updated to maximize distance from each other with L_{arc} . Consequently, all virtual prototypes converge to a single point in the feature space when trained with the original L_{arc} as shown in Fig. 3a. To address this problem, we propose to use virtual feature embedding $f'_{FR}(x_j)$ to update the virtual prototypes w_v^j . The virtual embedding $f'_{FR}(x_j)$ corresponding to virtual person ID: j was generated as follows:

$$f'_{FR}(x_j) = w_v^j + \mathcal{N}(0, 1) \cdot \sigma, \quad (5)$$

$$\sigma^2 = \frac{1}{b} \sum_{i=1}^b (f_{FR}(x_i) - w_r^i)^2, \quad (6)$$

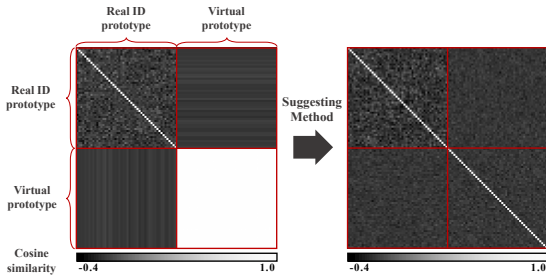
where b refers the mini-batch size. As can be seen from the equations, the virtual embedding $f'_{FR}(x_j)$ follows a distribution in which the standard deviation matches that of the real embeddings in a mini-batch. This virtual embedding enables the virtual prototype w_v^j to be updated while maintaining minimum similarities from other prototypes, as depicted in Fig. 3a. Since batch configuration impacts on the calculated standard deviation, we utilized Exponential Moving Average (EMA) to reduce this influence. Corrected standard deviation σ for current iteration t was computed as follows:

$$\sigma = \sigma_{(t)} \cdot \alpha + \sigma_{(t-1)} \cdot (1 - \alpha) \quad (7)$$

The hyperparameter α is set to 0.9. Each iteration, we generated virtual embeddings of the same size as the mini-batch b for training. Then, Eq. (3) is calculated using both virtual and real embeddings together. As shown in Fig. 3b, we confirm that the similarity distribution between virtual prototypes closely resembles the similarity distribution between real prototypes. Note that gradients for virtual embedding does not effect on the backbone, as shown in Fig. 2.

4.2 Stage 2: Face Synthesis with Diffusion Model

The next step is synthesizing face images using the diffusion model. To obtain the training dataset for the diffusion model, we utilize the FR model, which entails collecting pairs of images x_0 and their corresponding embeddings $f_{FR}(x_0)$. The input to our diffusion model includes the timestep t , the embedding vector $f_{FR}(x_0)$, and the noisy image x_t . In line with the approach proposed in the previous method [40], our model predicts clean images x_0 rather than noise ϵ injected into x_t . We adopt the U-ViT architecture [3] using the design approach of the visual transformer (ViT) [13]. We modify the U-ViT model by incorporating adaptive layer normalization (AdaLN), which shares similarities with the conditioning mechanism used in generative models [14, 35, 38]. Formally,



(a) Cosine similarity values between prototypes.

# ID	Condition	Mean (Std)
10K(Real) + 60K(Virtual)	R-R	0.009 (0.140)
	R-V	0.000 (0.044)
	V-V	0.010 (0.109)

(b) Means and standard deviations of cosine similarity values.

Fig. 3: The change of min-max normalized cosine similarity matrix of prototypes from our method. In the table, R and V represent the prototypes for real and virtual ID, respectively.

$\text{AdaLN}(h, c) = f_s(c)\text{LayerNorm}(h) + f_b(c)$, where h is the hidden states associated with the transformer block, and f_s, f_b are linear projections for condition embedding. In order to achieve both the generation of facial images and the synchronization of their feature space on the FR model, our diffusion model incorporates a constraint which aims to minimize the feature distance between the original image and the generated image as follows:

$$\min_{\theta} \mathbb{E}_{\epsilon, t} \|f_{\text{FR}}(\hat{x}_{\theta}(x_t, t, f_{\text{FR}}(x_0))) - f_{\text{FR}}(x_0)\|_2^2, \quad (8)$$

where $f_{\text{FR}}(x_0)$ indicates the FR model embedding for input image x_0 . We adopt classifier-free guidance [18] by randomly assigning zero values to condition embeddings $f_{\text{FR}}(x_0)$, *i.e.* the FR model embedding, 10% of the time. Sampling is performed as follows:

$$\tilde{x}_{\theta}(x_t, t, f_{\text{FR}}(x_0)) = w \cdot x_{\theta}(x_t, t, f_{\text{FR}}(x_0)) + (1 - w) \cdot x_{\theta}(x_t, t), \quad (9)$$

where $x_{\theta}(x_t, t, c)$ and $x_{\theta}(x_t, t)$ are conditional and unconditional x_0 -prediction, respectively and w is *guidance weight*. The pipeline of diffusion model is illustrated in the Appendix.

5 Experiments

We analyzed our framework from two perspectives. Firstly, by training the FR model exclusively with facial images generated from virtual IDs, we demonstrated the capability of our model to serve as a viable alternative to real face datasets, addressing concerns such as label noise or privacy. Secondly, we train the FR model using both real images and generated face images from virtual IDs, showcasing the potential of our model as a data augmentation framework for face recognition.

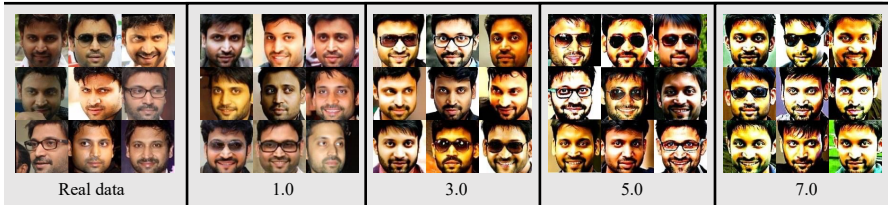


Fig. 4: Generated images of real ID with different classifier-free guidance weights. Higher guidance weights enforce stronger conditioning of input labels but slightly similar samples. However, a high guidance weight results in over-enhanced images.

5.1 Implementation Details

For stage 1: All experiments share the same implementation details for stage 1, with the only difference being the use of the virtual embedding $f'_{\text{FR}}(x_j)$ during training. Modified ResNet-50 [10] and ArcFace [10] were employed for training the FR backbone. CASIA-WebFace [21] and MS1M-V2 [10] datasets were used for training. Following the approach in [30], the faces were aligned resulting in an image size of 112×112 . After the alignment, the pixel values of the training dataset were normalized, setting the mean and standard deviation at 0.5 each. The size of the mini-batch was set to 512, and Stochastic Gradient Descent (SGD) was used as the optimizer. The weight decay was set at $5e-4$ and the momentum at 0.9. The initial learning rate was set at 0.1. We divided our training protocol into two, depending on the training dataset. When training the model with CASIA-WebFace dataset, the learning rate decayed by 0.1 at the 24th, 30th, and 36th epochs, and training terminated after the 40th epoch. The hyperparameters for the margin m and scale factor s in Eq. (3) were set to 0.5 and 30, respectively. When training the model with the MS1M-V2 dataset, we decayed the learning rate by 0.1 at the 10th, 18th, and 22nd epochs and terminated the training after the 25th epoch. The hyperparameters for the margin m and scale factor s in Eq. (3) were set to 0.5 and 64, respectively, when training with the MS1M-V2 dataset.

For stage 2: To generate synthetic face images, we explored the best setting for the diffusion model. To facilitate comparison, we utilized the widely adopted ViT-B model for all experiments. Since the traditional FR model typically employs a resolution of 112×112 for face images, we set the window size of the ViT patch extractor to 4. We followed the publicly released implementation of DDIM [47] with the cosine noise scheduler [7]. The diffusion model was trained for 5M iterations with a batch size of 512 using AdamW Optimizer [29, 32] with a learning rate of $1e-4$. For sampling, we used classifier-free guidance implementation [18] in 100 timesteps.

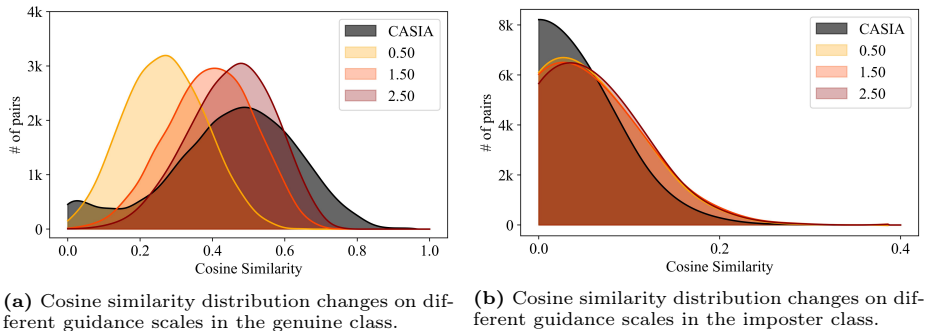


Fig. 5: Data distributions of the real and our proposed generated data.

CFG scale	0.5	1.0	1.5	2.0	2.5	3.0
Genuine	0.88	0.90	0.83	0.81	0.81	0.81
Imposter	0.93	0.89	0.87	0.83	0.76	0.76
Average	0.90	0.89	0.85	0.82	0.78	0.73

(a) IoU of the similarity distributions between real and synthesized images for real ID.

CFG scale	0.5	1.0	1.5	2.0	2.5	3.0
Genuine	0.28	0.40	0.51	0.60	0.65	0.68
Imposter	0.81	0.77	0.79	0.77	0.77	0.73
Average	0.54	0.78	0.65	0.68	0.71	0.70

(b) IoU of the similarity distributions between real and synthesized images for virtual ID.

Table 1: Impact of classifier-free guidance scale on similarity among the genuine (positive pair) and imposter (negative pair), respectively. We evaluate the IoU between the distributions of synthesized and real images on different guidance scales.

5.2 Virtual Identity Generation

Since diffusion models focus on optimizing the visual aspect with input conditions, they tend to produce images that are high in consistency but lack of variance. One simple way to achieve a balance between consistency and variance is by adjusting the classifier-free guidance weight scale. Higher guidance enforces stronger conditioning of input labels but slightly similar samples, as shown in Fig. 4. However, it is evident that a high guidance weight results in over-enhanced images. To effectively generate constant but diverse face images, we evaluate the similarity between the synthesized images and compare their distributions with real data on different guidance scales. In Fig. 5, we illustrate the similarity distributions of our generated images and real images as predicted by pre-trained ResNet-18 models trained with ArcFace [10] and Glint-360K [1]. As shown in the figure, a higher weight causes the similarity distribution to shift towards higher average. In other words, a higher guidance weight results in more constant images. To determine the optimal scale for replicating the real data distribution, we assess the Intersection over Union (IoU) between the distributions of real and synthetic data. Note that the similarity distributions of real ID and virtual ID exhibit distinct patterns on the guidance scale, as shown in Tab. 1. We observe that the proposed model simulates the actual data distribution for the real ID when the scale is $w = 0.5$, but the synthesis of the virtual ID performs best as the scale becomes $w = 2.5$.



Fig. 6: Comparison of the generated virtual ID images with the conventional methods [2, 28, 39] and our methods that are trained on CASIA-WebFace and MS1M-V2. Each row shows samples from the same ID.

We construct a toy example visualizing the embeddings of three real persons and five generated virtual persons to demonstrate the efficacy of the synthesized images in Fig. 1. As seen on the left figure, the virtual embedding optimization obviously provides separable virtual prototypes from real individual clusters. The right figure illustrates that our synthesized images enforce high intra-class variance. Synthesized images of real individuals filling the gap in the cluster provide variance to the subjects. Additionally, the cluster of generated images from virtual ID prototypes, while staying separate from other subjects, demonstrates the effectiveness of our framework for generating unique virtual human faces in high consistency.

We compare the synthetic face images of virtual ID with the conventional methods in Fig. 6. Each row is sampled from the same individual. Since DigiFace [2] synthesizes virtual human faces using 3D digital modeling, it fails to match the distribution of real face images in terms of appearance as depicted in the figure. Although SynFace [39] produces facial images of high quality and consistency, it has limitations in separability, leading to the generation of a restricted set of unique individuals, fewer than 500 [28]. On the other hand, DCFace [28] demonstrates different scenarios for the same person, but struggles to maintain uniformity. Generated facial images using VIGFace model demonstrates remarkable uniformity in generating consistent virtual individuals, while also in-



Fig. 7: Generated real ID images of our MS1M-V2 trained model. We note that we report subjects with only two images in the original dataset. This shows that our method can generate diverse conditions even with a limited number of images.

incorporating variations such as hair styles, glasses, makeup, and age. Note that the important characteristic of a training dataset to achieve a high-performance FR model is not the high quality of the images themselves, but rather the high consistency and variance of the generated facial images belonging to one person.

Fig. 7 illustrates the synthesized results of real ID trained on MS1M-V2. Note that we report subjects which only contains few number (only 2) of images in the original dataset. Since the lack of variance in the class introduces considerable bias into the training process, increasing the variance within the class is crucial. The results demonstrate that the proposed approach is capable of producing diverse conditions even when working with a small number of images without any help from external data.

Property of generated Dataset To investigate the properties of the generated images, we measured the 1) intra-class consistency, 2) intra-class variance, and 3) inter-class separability of generated images. The intra-class consistency indicates how consistent the samples are in adhering to the label condition. Consequently, the consistency of class k (CST_k) was measured as follows:

$$\text{CST}_k = \frac{1}{N^2} \sum_{j=1}^N \sum_{i=1}^N \frac{f(x_i)f(x_j)}{\|f(x_i)\|\|f(x_j)\|}, \quad (10)$$

where N is the number of images in a class k . Higher intra-class consistency means that the similarities between samples under the same subject are high. The intra-class diversity measures how various the conditions of samples are under the same label condition. Various conditions, such as pose, low light, and occlusions, make face recognition more challenging. Motivated by this observation, we calculated the intra-class diversity of a class k (DIV_k) using the variance of Face Image Quality Assessment (FIQA) scores as follows:

$$\text{DIV}_k = \frac{1}{N} \sum_{i=1}^N (\text{FIQA}(x_i) - \overline{\text{FIQA}(x_i)})^2, \quad (11)$$

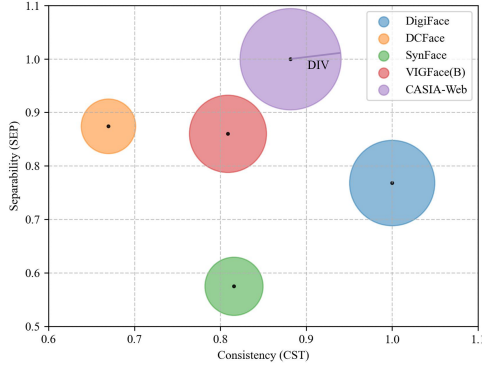


Fig. 8: The normalized intra-class consistency (CST) versus inter-class separability (SEP) graph of various methods. The sizes of circles indicate the intra-class diversities (DIV).

$$\overline{\text{FIQA}(x_i)} = \frac{1}{N} \sum_{i=1}^N \text{FIQA}(x_i), \quad (12)$$

where $\text{FIQA}(x_i)$ indicates the SER-FIQ score [50] of the generated image x_i . We also measured the inter-class separability to assess the integrity of the dataset; in other words, to ensure that all subjects in the dataset are unique. Inspired by [5], the inter-class separability for a class k (SEP_k) is measured based on the class center angular similarity (CCS) and the nearest negative class center angular similarity (NNCCS) as follows:

$$\text{SEP}_k = \frac{1}{N} \sum_{i=1}^N \frac{\text{CCS}_{x_i}}{\text{NNCCS}_{x_i}}, \quad (13)$$

$$\text{CCS}_{x_i} = \frac{f(x_i) \overline{f(x_i)}}{\|f(x_i)\| \|\overline{f(x_i)}\|}, \text{NNCCS}_{x_i} = \max_{j \in \{1, \dots, C\}, j \neq i} \frac{f(x_i) \overline{f(x_j)}}{\|f(x_i)\| \|\overline{f(x_j)}\|}, \quad (14)$$

where $\overline{f(x_i)}$ represents the class center obtained by averaging the embedding vectors of the generated image x_i under the same class. As shown in the formula, a high SEP_k indicates that the generated images are closer to the center than to the nearest negative class center. The scores, CST_k , DIV_k , and SEP_k , are derived from a pretrained ArcFace model that was trained using the Glint-360K dataset. Fig. 8 plots the average values of the properties for all classes. VIGFace shows balanced scores in terms of intra-class consistency, intra-class variance, and inter-class separability compared to other methods. DCFace, the SOTA model that also utilizes a diffusion model, exhibits similar separability, but lower consistency compared to VIGFace. DigiFace achieves the highest consistency, due to its utilization of 3D rendering methods, but its image style may

Training Dataset	# of Images (classes \times variations)	Accuracy on Benchmark Dataset					Average Accuracy	GR (%)
		LFW	CFP-FP	CPLFW	AgeDB	CALFW		
CASIA-Webface (Real)	0.49M ($\approx 10.5K \times 47$)	99.35	95.97	84.12	93.65	90.78	92.77	-
SynFace	0.5M ($10K \times 50$)	84.10	70.06	59.42	63.00	63.93	68.10	36.2
DigiFace	1.2M ($10K \times 72 + 100K \times 5$)	85.22	75.33	60.35	61.72	61.80	68.88	34.7
DCFace	1.2M ($20K \times 50 + 40K \times 5$)	98.42	84.53	76.67	89.78	88.95	87.67	5.8
VIGFace(S)	0.5M ($10K \times 50$)	96.60	86.66	75.03	82.50	83.42	84.84	9.3
VIGFace(B)-LT	1.2M ($20K \times 50 + 40K \times 5$)	98.30	90.60	79.88	88.63	87.50	88.98	4.3
VIGFace(B)	1.2M ($60K \times 20$)	98.45	92.07	80.15	89.82	88.43	89.78	3.3
VIGFace(L)	2.4M ($120K \times 20$)	98.65	93.47	83.68	90.55	90.10	91.29	1.6
VIGFace(H)	4.2M ($60K \times 50 + 60K \times 20$)	99.13	91.87	84.83	94.63	93.38	92.77	0.0

Table 2: FR benchmark results trained with various synthesized datasets. The 1:1 verification accuracies(%) of the famous five benchmarks are reported. We specify our method according to the image and subject sizes as small(S), base(B), large(L), and huge(H). All datasets are generated based on CASIA-Webface, except for (H), which is based on MS1M-V2.

differ significantly from real datasets, leading to lower accuracy in real-world applications. SynFace shows similar consistency as ours but has the lowest separability due to its mix-up generation method.

5.3 Evaluation

VIGFace as a Virtual Dataset We compared the performance of the FR model trained with generated facial images from virtual IDs using VIGFace with conventional methods: SynFace [39], DigiFace [2], and DCFace [28]. For the experiment, we set the number of virtual IDs to 60K and 120K. To ensure a valid comparison, we establish image counts of 0.5M and 1.2M, representing the scale of the real CASIA-WebFace dataset and previous synthetic approaches, respectively. In Tab. 2, we present the 1:1 verification accuracy (%) on five benchmarks [22, 36, 45, 56, 57]. The last column is calculated using the average performance of five benchmarks to represent the FR performance gap from the FR model trained with the real dataset, as suggested in [28]. Gap-to-Real (GR) is calculated as $GR = (Average_{real} - Average_{syn}) / Average_{syn}$. GRs are calculated using the performance of CASIA-WebFace. From the table, it is evident that DCFace achieves a superior performance among conventional methods. However, VIGFace(B) shows comparable or slightly better performance than the previous state-of-the-art method on the LFW, AgeDB, and CALFW datasets, while demonstrating superior improvement on the CFP-FP and CPLFW datasets. This indicates that our methods can generate virtual IDs with more diverse pose variations while maintaining ID consistency. When the FR model was trained using VIGFace(B), it achieved a GR of 3.3%, and a large set VIGFace(L) achieved a GR of only 1.6%. This proves that the model trained with VIGFace can achieve FR performance close to that of FR models trained with a real dataset. Note that the FR model trained with VIGFace(H), *i.e.* generated using MS1M-V2, achieves the same verification accuracy as the model trained with the real CASIA-WebFace. This indicates that our virtual dataset can completely replace the CASIA-WebFace dataset to train the FR model without any privacy issues.

Training Dataset	# of Images	Accuracy on Benchmark Dataset					Average Accuracy
		LFW	CFP-FP	CPLFW	AgeDB	CALFW	
Real	0.49M	99.35	95.97	84.12	93.65	90.78	92.77
+SynFace	0.5M	99.38	96.03	84.15	93.38	90.68	92.72 (−0.05)
+DCFFace	1.2M	99.38	95.90	83.63	93.53	90.58	92.60 (−0.17)
+VIGFace	1.2M	99.50	96.93	86.20	94.78	92.05	93.89 (+1.12)

Table 3: FR benchmark results of FR models that trained using both of real and synthetic datasets. The 1:1 verification accuracies (%) are reported for the famous five benchmarks. We utilize VIGFace(B) in this experiment.

VIGFace for Data Augmentation To demonstrate the efficacy of VIGFace as an augmentation framework, we evaluate the accuracy of the FR model trained with both real and virtual ID face images. Tab. 3 shows the performance change of the trained FR model utilizing various combinations of datasets. As depicted in the table, the FR model that was trained with a combination of real data and virtual images produced by VIGFace exhibits enhanced performance across all benchmarks in comparison to the model trained solely on real data. This contrasts with the performance decline of the model using conventional synthetic datasets as an augmentation method. The results of our experiment indicate that the proposed method can accurately mirror the real facial data to blend and make synergy with them. Consequently, VIGFace not only effectively solves the privacy issue, but also can be used with real data for FR training to help achieve better generalization and high performance, which conventional methods cannot.

6 Conclusions

This paper presents a simple yet effective method for creating a synthetic dataset that guarantees the unique virtual identities. Synthesized facial data can serve as a solution for various challenges faced by traditional real datasets, such as high expenses, inaccuracies and biases in labeling, and concerns regarding privacy. To this end, we propose the Virtual Identity Generation framework and demonstrate that it can generate realistic and diverse facial images of virtual individuals, significantly narrowing the performance gap with FR models trained on real data. Furthermore, the model exhibits superior performance when trained on a combination of data from VIGFace and existing real data compared to models trained solely on real data. This confirms that our proposed method has potential as an effective augmentation technique. We will publicly distribute the virtual face dataset created by VIGFace and believe that this new virtual data will contribute to resolving the privacy issues inherent in face recognition training dataset.

References

1. An, X., Zhu, X., Gao, Y., Xiao, Y., Zhao, Y., Feng, Z., Wu, L., Qin, B., Zhang, M., Zhang, D., et al.: Partial fc: Training 10 million identities on a single machine. In: Proceedings of the IEEE/CVF International Conference on Computer Vision. pp. 1445–1449 (2021)
2. Bae, G., de La Gorce, M., Baltrušaitis, T., Hewitt, C., Chen, D., Valentin, J., Cipolla, R., Shen, J.: Digiface-1m: 1 million digital face images for face recognition. In: Proceedings of the IEEE/CVF Winter Conference on Applications of Computer Vision. pp. 3526–3535 (2023)
3. Bao, F., Nie, S., Xue, K., Cao, Y., Li, C., Su, H., Zhu, J.: All are worth words: A vit backbone for diffusion models. In: Proceedings of the IEEE/CVF Conference on Computer Vision and Pattern Recognition. pp. 22669–22679 (2023)
4. Boutros, F., Damer, N., Kirchbuchner, F., Kuijper, A.: Elasticface: Elastic margin loss for deep face recognition. In: Proceedings of the IEEE/CVF conference on computer vision and pattern recognition. pp. 1578–1587 (2022)
5. Boutros, F., Fang, M., Klemm, M., Fu, B., Damer, N.: Cr-fiq: Face image quality assessment by learning sample relative classifiability. In: Proceedings of the IEEE/CVF Conference on Computer Vision and Pattern Recognition (CVPR). pp. 5836–5845 (June 2023)
6. van Breugel, B., Kyono, T., Berrevoets, J., van der Schaar, M.: Decaf: Generating fair synthetic data using causally-aware generative networks. *Advances in Neural Information Processing Systems* **34**, 22221–22233 (2021)
7. Chen, T.: On the importance of noise scheduling for diffusion models. *arXiv preprint arXiv:2301.10972* (2023)
8. Cho, H., Park, H., Kim, I.J., Cho, J.: Data augmentation of backscatter x-ray images for deep learning-based automatic cargo inspection. *Sensors* (2021)
9. Deng, J., Guo, J., Liu, T., Gong, M., Zafeiriou, S.: Sub-center arcface: Boosting face recognition by large-scale noisy web faces. In: *Computer Vision–ECCV 2020: 16th European Conference, Glasgow, UK, August 23–28, 2020, Proceedings, Part XI* 16. pp. 741–757. Springer (2020)
10. Deng, J., Guo, J., Xue, N., Zafeiriou, S.: Arcface: Additive angular margin loss for deep face recognition. In: Proceedings of the IEEE/CVF conference on computer vision and pattern recognition. pp. 4690–4699 (2019)
11. Deng, J., Guo, J., Yang, J., Lattas, A., Zafeiriou, S.: Variational prototype learning for deep face recognition. In: Proceedings of the IEEE/CVF Conference on Computer Vision and Pattern Recognition. pp. 11906–11915 (2021)
12. Deng, Y., Yang, J., Chen, D., Wen, F., Tong, X.: Disentangled and controllable face image generation via 3d imitative-contrastive learning. In: Proceedings of the IEEE/CVF conference on computer vision and pattern recognition. pp. 5154–5163 (2020)
13. Dosovitskiy, A., Beyer, L., Kolesnikov, A., Weissenborn, D., Zhai, X., Unterthiner, T., Dehghani, M., Minderer, M., Heigold, G., Gelly, S., et al.: An image is worth 16x16 words: Transformers for image recognition at scale. *arxiv 2020. arXiv preprint arXiv:2010.11929* (2010)
14. Dumoulin, V., Shlens, J., Kudlur, M.: A learned representation for artistic style. In: *International Conference on Learning Representations* (2016)
15. Guo, Y., Zhang, L., Hu, Y., He, X., Gao, J.: Ms-celeb-1m: A dataset and benchmark for large-scale face recognition. In: *Computer Vision–ECCV 2016: 14th European Conference, Amsterdam, The Netherlands, October 11–14, 2016, Proceedings, Part III* 14. pp. 87–102. Springer (2016)

16. He, K., Zhang, X., Ren, S., Sun, J.: Delving deep into rectifiers: Surpassing human-level performance on imagenet classification. In: Proceedings of the IEEE international conference on computer vision. pp. 1026–1034 (2015)
17. He, K., Zhang, X., Ren, S., Sun, J.: Deep residual learning for image recognition. In: Proceedings of the IEEE conference on computer vision and pattern recognition. pp. 770–778 (2016)
18. Ho, J., Salimans, T.: Classifier-free diffusion guidance. In: NeurIPS 2021 Workshop on Deep Generative Models and Downstream Applications (2021)
19. Hong, J.H., Kim, H., Kim, M., Nam, G.P., Cho, J., Ko, H.S., Kim, I.J.: A 3d model-based approach for fitting masks to faces in the wild. In: 2021 IEEE International Conference on Image Processing (ICIP) (2021)
20. Hu, J., Shen, L., Sun, G.: Squeeze-and-excitation networks. In: Proceedings of the IEEE conference on computer vision and pattern recognition. pp. 7132–7141 (2018)
21. Huang, G., Mattar, M., Lee, H., Learned-Miller, E.: Learning to align from scratch. *Advances in neural information processing systems* **25** (2012)
22. Huang, G.B., Mattar, M., Berg, T., Learned-Miller, E.: Labeled faces in the wild: A database for studying face recognition in unconstrained environments. In: Workshop on faces in 'Real-Life' Images: detection, alignment, and recognition (2008)
23. Huang, Y., Wang, Y., Tai, Y., Liu, X., Shen, P., Li, S., Li, J., Huang, F.: Curricular-face: adaptive curriculum learning loss for deep face recognition. In: proceedings of the IEEE/CVF conference on computer vision and pattern recognition. pp. 5901–5910 (2020)
24. Hwang, H., Jang, C., Park, G., Cho, J., Kim, I.J.: Eldersim: A synthetic data generation platform for human action recognition in eldercare applications. *IEEE Access* (2023)
25. Ioffe, S., Szegedy, C.: Batch normalization: Accelerating deep network training by reducing internal covariate shift. In: International conference on machine learning. pp. 448–456. pmlr (2015)
26. Kemelmacher-Shlizerman, I., Seitz, S.M., Miller, D., Brossard, E.: The megaface benchmark: 1 million faces for recognition at scale. In: Proceedings of the IEEE conference on computer vision and pattern recognition. pp. 4873–4882 (2016)
27. Kim, M., Jain, A.K., Liu, X.: Adaface: Quality adaptive margin for face recognition. In: Proceedings of the IEEE/CVF conference on computer vision and pattern recognition. pp. 18750–18759 (2022)
28. Kim, M., Liu, F., Jain, A., Liu, X.: Dcfacer: Synthetic face generation with dual condition diffusion model. In: Proceedings of the IEEE/CVF Conference on Computer Vision and Pattern Recognition. pp. 12715–12725 (2023)
29. Kinga, D., Adam, J.B., et al.: A method for stochastic optimization. In: International conference on learning representations (ICLR). vol. 5, p. 6. San Diego, California; (2015)
30. Liu, W., Wen, Y., Yu, Z., Li, M., Raj, B., Song, L.: Sphreface: Deep hypersphere embedding for face recognition. In: Proceedings of the IEEE conference on computer vision and pattern recognition. pp. 212–220 (2017)
31. Liu, Y., Liu, X.: Spoof trace disentanglement for generic face anti-spoofing. *IEEE Transactions on Pattern Analysis and Machine Intelligence* **45**(3), 3813–3830 (2022)
32. Loshchilov, I., Hutter, F.: Decoupled weight decay regularization. *arXiv preprint arXiv:1711.05101* (2017)
33. Van der Maaten, L., Hinton, G.: Visualizing data using t-sne. *Journal of machine learning research* **9**(11) (2008)

34. Meng, Q., Zhao, S., Huang, Z., Zhou, F.: Magface: A universal representation for face recognition and quality assessment. In: Proceedings of the IEEE/CVF conference on computer vision and pattern recognition. pp. 14225–14234 (2021)
35. Miyato, T., Koyama, M.: cgans with projection discriminator. In: International Conference on Learning Representations (2018)
36. Moschoglou, S., Papaioannou, A., Sagonas, C., Deng, J., Kotsia, I., Zafeiriou, S.: Agedb: the first manually collected, in-the-wild age database. In: proceedings of the IEEE conference on computer vision and pattern recognition workshops. pp. 51–59 (2017)
37. Nech, A., Kemelmacher-Shlizerman, I.: Level playing field for million scale face recognition. In: Proceedings of the IEEE Conference on Computer Vision and Pattern Recognition. pp. 7044–7053 (2017)
38. Preechakul, K., Chatthee, N., Wizadwongsa, S., Suwajanakorn, S.: Diffusion autoencoders: Toward a meaningful and decodable representation. In: Proceedings of the IEEE/CVF Conference on Computer Vision and Pattern Recognition. pp. 10619–10629 (2022)
39. Qiu, H., Yu, B., Gong, D., Li, Z., Liu, W., Tao, D.: Synface: Face recognition with synthetic data. In: Proceedings of the IEEE/CVF International Conference on Computer Vision. pp. 10880–10890 (2021)
40. Ramesh, A., Dhariwal, P., Nichol, A., Chu, C., Chen, M.: Hierarchical text-conditional image generation with clip latents. arXiv preprint arXiv:2204.06125 1(2), 3 (2022)
41. Rombach, R., Blattmann, A., Lorenz, D., Esser, P., Ommer, B.: High-resolution image synthesis with latent diffusion models. In: Proceedings of the IEEE/CVF conference on computer vision and pattern recognition. pp. 10684–10695 (2022)
42. Saharia, C., Chan, W., Saxena, S., Li, L., Whang, J., Denton, E.L., Ghasemipour, K., Gontijo Lopes, R., Karagol Ayan, B., Salimans, T., et al.: Photorealistic text-to-image diffusion models with deep language understanding. *Advances in Neural Information Processing Systems* **35**, 36479–36494 (2022)
43. Sankaranarayanan, S., Alavi, A., Castillo, C.D., Chellappa, R.: Triplet probabilistic embedding for face verification and clustering. In: 2016 IEEE 8th international conference on biometrics theory, applications and systems (BTAS). pp. 1–8. IEEE (2016)
44. Schroff, F., Kalenichenko, D., Philbin, J.: Facenet: A unified embedding for face recognition and clustering. In: Proceedings of the IEEE conference on computer vision and pattern recognition. pp. 815–823 (2015)
45. Sengupta, S., Chen, J.C., Castillo, C., Patel, V.M., Chellappa, R., Jacobs, D.W.: Frontal to profile face verification in the wild. In: 2016 IEEE winter conference on applications of computer vision (WACV). pp. 1–9. IEEE (2016)
46. Simonyan, K., Zisserman, A.: Very deep convolutional networks for large-scale image recognition. arXiv preprint arXiv:1409.1556 (2014)
47. Song, J., Meng, C., Ermon, S.: Denoising diffusion implicit models. arXiv preprint arXiv:2010.02502 (2020)
48. Srivastava, N., Hinton, G., Krizhevsky, A., Sutskever, I., Salakhutdinov, R.: Dropout: a simple way to prevent neural networks from overfitting. *The journal of machine learning research* **15**(1), 1929–1958 (2014)
49. Sun, Y., Liu, Y., Liu, X., Li, Y., Chu, W.S.: Rethinking domain generalization for face anti-spoofing: Separability and alignment. In: Proceedings of the IEEE/CVF Conference on Computer Vision and Pattern Recognition. pp. 24563–24574 (2023)

50. Terhörst, P., Kolf, J.N., Damer, N., Kirchbuchner, F., Kuijper, A.: Ser-fiq: Unsupervised estimation of face image quality based on stochastic embedding robustness. In: CVPR. vol. 1, p. 2 (2020)
51. Tremblay, J., Prakash, A., Acuna, D., Brophy, M., Jampani, V., Anil, C., To, T., Cameracci, E., Bochoon, S., Birchfield, S.: Training deep networks with synthetic data: Bridging the reality gap by domain randomization. In: Proceedings of the IEEE conference on computer vision and pattern recognition workshops. pp. 969–977 (2018)
52. Van Noord, R.: The ethical questions that haunt facial-recognition research. *Nature* **587**(7834), 354–359 (2020)
53. Wang, H., Wang, Y., Zhou, Z., Ji, X., Gong, D., Zhou, J., Li, Z., Liu, W.: Cosface: Large margin cosine loss for deep face recognition. In: Proceedings of the IEEE conference on computer vision and pattern recognition. pp. 5265–5274 (2018)
54. Wen, Y., Zhang, K., Li, Z., Qiao, Y.: A discriminative feature learning approach for deep face recognition. In: Computer Vision–ECCV 2016: 14th European Conference, Amsterdam, The Netherlands, October 11–14, 2016, Proceedings, Part VII 14. pp. 499–515. Springer (2016)
55. Yi, D., Lei, Z., Liao, S., Li, S.Z.: Learning face representation from scratch. arXiv preprint arXiv:1411.7923 (2014)
56. Zheng, T., Deng, W.: Cross-pose lfw: A database for studying cross-pose face recognition in unconstrained environments. Beijing University of Posts and Telecommunications, Tech. Rep **5**(7) (2018)
57. Zheng, T., Deng, W., Hu, J.: Cross-age lfw: A database for studying cross-age face recognition in unconstrained environments. arXiv preprint arXiv:1708.08197 (2017)
58. Zhu, Z., Huang, G., Deng, J., Ye, Y., Huang, J., Chen, X., Zhu, J., Yang, T., Lu, J., Du, D., et al.: Webface260m: A benchmark unveiling the power of million-scale deep face recognition. In: Proceedings of the IEEE/CVF Conference on Computer Vision and Pattern Recognition. pp. 10492–10502 (2021)